Tri-plane cardiac imaging using multi-line transmission on a spiral array: a feasibility study

Alessandro Ramalli[1,2], Pedro Santos[1], Piero Tortoli[2], Jan D'hooge[1]

[1]*Lab. on Cardiovascular Imaging & Dynamics, Dept. of Cardiovascular Sciences, KU Leuven,* Leuven, Belgium

[2]*Department of Information Engineering, University of Florence,* Florence, Italy

***Abstract*— The assessment of regional cardiac function requires imaging all segments of the left ventricle. Since full 3D echocardiography remains limited in space-time resolution, tri-plane imaging has been proposed as an intermediate solution to alleviate such problem. Although its time resolution was further improved by a multi-line transmission (MLT) scheme, its implementation resulted impractical since it requires a fully wired 32×32 array. The aim of this study was therefore to test the feasibility of MLT-based tri-plane imaging using a 2D array with low element count.**

A spiral array (SA) was designed based on a 32×32 full array (FA); both SA and FA were simulated in Field II and their performance compared in terms of 3D one-way pressure fields when used in tri-plane imaging modality. Both probes performed similarly in terms of lateral resolution (2.4 mm) and depth of field (>37 mm) but, as expected, the SA presented lower sensitivity (-13.7dB) and worse grating-lobe level (+5.6dB); correspondingly, SA reduces the image contrast ratio (-9.2dB) and contrast-to-noise ratio (-20%). On the other hand, the SA slightly improved the speckle signal-to-noise ratio (+7%) thus increasing the homogeneity of the background region. In conclusion, despite an unavoidable loss in image quality, tri-plane imaging using MLT using a SA seems feasible.

Keywords*— *Spiral array, high frame rate, cardiac imaging, multiplane imaging.

I. Introduction

Echocardiography, among the other imaging modalities, is appreciated for its bedside applicability, temporal resolution, real-time operation, low cost and absence of ionizing radiation. Although 2D ultrasound (US) imaging is still the most used modality, 3D echocardiography has recently matured as a clinical imaging technique and it is currently implemented in the flagship scanners of some US companies. However, morphological and functional characterization of the heart of an individual patient using the current 3D technology remains limited [1]–[3]. Indeed, variability of most of the quantitative measurements remains high, due to the relatively low spatio-temporal resolution obtained with conventional acquisition schemes, which require spatial stitching of several sub volumes recorded from different cardiac cycles and synchronized through the electrocardiogram (ECG) signal.

As full 3D echocardiography is limited in space-time resolution, tri-plane imaging, e.g. the simultaneous imaging of three cross-sections of the heart, has been proposed. In addition, its time resolution was further improved by a multi-line transmission (MLT) scheme [4]–[6], i.e. a high frame rate imaging method, that exploits the simultaneous transmission of multiple focused beams along different directions to increase the frame rate by a factor equal to the number of MLT beams [7]–[9]. However, the implementation of MLT tri-plane imaging, as proposed in [5], is still impractical: it requires fully sampled matrix arrays that should include thousands of small elements, which makes impractical the implementation of the entire ultrasound system, i.e. probe, connection cable, and scanner [10]. A solution to reduce this problem is represented by sparse array probes [11]–[16]; this approach directly reduces the number of transducers by reducing the array sampling while optimizing the position of each single transducer element.

Therefore, the aim of this study was to test the feasibility of MLT-based tri-plane imaging using a 2D array with low element count (<256). Hereby, a spiral array was designed based on a 32×32 full array; both the arrays were simulated in Field II [17], [18] and their performance compared in terms of 3D one-way pressure fields and tri-plane imaging capability.

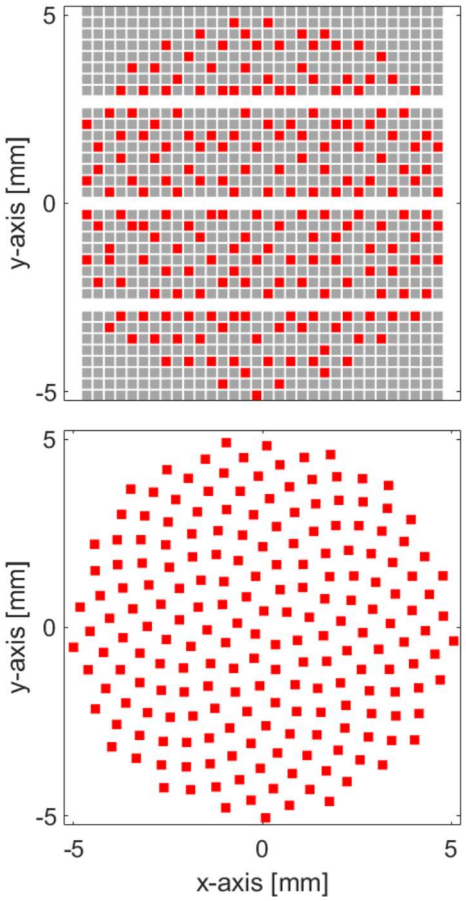

Fig. 1 Layout of the arrays. Top: in gray, the elements belonging to the full-array (FA) only; in red, the elements belonging to both the full-array and the spiral-array (SA). Bottom: the ungridded, uniform, 10mm-wide spiral with 200 seeds that was adapted on FA to obtain SA.

This work was supported by the European Union's Horizon 2020 research and innovation programme under the Marie Skłodowska-Curie grant agreement No 786027 (ACOUSTIC project).

DOI: 10.1109/ULTSYM.2018.8580143

The paper is organized as follows: section II presents the full array layout as well as the design method used for the spiral array; moreover, it presents the setups for the one-way field and tri-plane imaging simulations; section III shows simulation results and compares the performance of the two arrays; section IV concludes the paper.

II. Materials & Methods

A. System and arrays

The High channel Density Programmable ULtrasound System based on consumer Electronics (HD-PULSE) [19] is a modular, scalable, generic and fully programmable ultrasound platform. The system has 256 independent channels in both transmission and reception, connected to 1:4 multiplexers to control 2D matrix array transducer having up to 1024 elements.

The full-array (FA) was simulated based on the characteristics of the 2D matrix array (Vermon S.A., Tours, France) available at the Lab. on Cardiovascular Imaging & Dynamics. It consists of 32 (x-axis) by 35 (y-axis) elements (3 MHz, 300 µm pitch, 70% bandwidth), but on the y-direction one row every nine is not connected, hence the total number of elements is 1024 [20], [21], see Fig. 1 for the actual active layout.

A spiral array (SA) was designed based on the gridded layout of FA and considering the characteristics of the multiplexer, i.e. considering that each channel of the system is assigned to one group of 4 consecutive elements along the y-direction. The design was based on an ungridded, uniform, 10mm-wide spiral with 200 seeds [14], see Fig. 1 bottom for its ideal layout. The elements belonging to SA (Fig. 1 top) were selected among those of FA, by activating the available elements whose positions were closest to the ideal positions of the ungridded spiral.

B. Simulations & performance metrics

1) One-way fields

Three-dimensional one-way fields radiated by FA and SA were simulated by Field II. For each array, 81 steering angles were simulated, i.e. the combinations of 9 uniformly spaced angles between −40° and 40° in both elevation and azimuth planes. The emitted pressure was simulated in a 151×151×61-point matrix, corresponding to a 100×100×40 mm^3 box along the x, y and z directions, respectively. The box was centered at (0,0,40) mm. The simulated one-way fields were further elaborated in order to extract the grating-lobe-level (GLL), the sensitivity (S), the depth of field (DoF), and the lateral resolution (LR). S was estimated as the normalized focal intensity, assuming as reference the intensity radiated by FA when no steering was applied. GLL was estimated as the ratio between the intensity of the highest secondary lobe and the main lobe intensity. DoF was assessed as the −6dB beam length along the beam direction; while LR was computed as the average −6dB width of the main beam (full width half maximum - FWHM) in the plane perpendicular to the US propagation direction.

2) MLT Tri-plane imaging

Tri-plane images were simulated using both FA and SA. The 3 reconstructed B-mode images were positioned at rotational angles of 0°, 90° and 45°, respectively (Fig. 2); each one covered a region of interest 80°-wide, scanned in nL=101 lines. For MLT imaging, $nMLT$=3 beams were simultaneously transmitted; each of the beams scanned only one out of the 3 reconstructed planes. Moreover, in order to limit the cross-talk among beams, an alternated pattern scheme was implemented as sketched in Fig. 3. In particular, for the n-th transmission event ($n \in [1, nL]$), the b-th beam ($b \in [1, nMLT]$) was transmitted along the image-plane line number

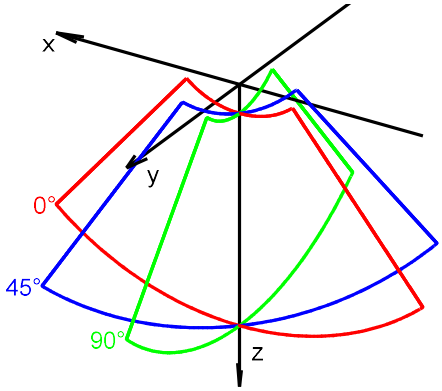

Fig. 2 The reference system and the reconstructed regions of interest. The probe is centered on the origin of the reference system. Tri-plane images are reconstructed at different rotational angles 0° (red), 90° (green) and 45° (blu), respectively.

$$l_b(n) = 1 + \left\{ \left[\left\lfloor \frac{(b-1)\cdot nL}{nMLT} \right\rceil + n - 1 \right] \% \, nL \right\} \quad (1)$$

where $\lfloor \cdot \rceil$ is the round to the closest integer operator and % is the modulus operator.

A numerical phantom was developed for assessment of the imaging performance; it consisted of a uniform distribution of scatterers in a 80×80×30 mm^3 box containing a 10-mm wide, spherical, anechoic inclusion. The density of scatterers was fixed at 2000 scatterers per cm^3 and the phantom was centered at (0, 0, 40 mm). The imaging performance was then quantified by contrast ratio (CR), contrast-to-noise ratio (CNR) and speckle signal-to-noise ratio (sSNR), defined as follows:

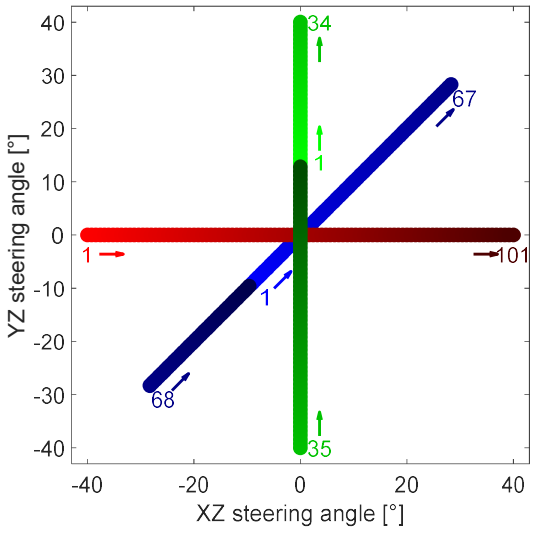

Fig. 3 Tri-plane alternated scan sequence. Beam 1 (red), 2 (green), 3 (blu) respectively scan the planes at rotational angles 0°, 90° and 45°. Arrows indicate the scan direction; the numbers correspond to the transmission event index (n) for which the beams reach the borders of their respective scan plane. Moreover, "1s" highlight the position of the beams at the first transmission event.

$$\mathrm{CR} = \frac{\int_{C_{ROI}} dS}{\int_{S_{ROI}} dS} \cdot \frac{\int_{S_{ROI}} |IQ(S)|^2 \, dS}{\int_{C_{ROI}} |IQ(S)|^2 \, dS} \tag{2}$$

$$\mathrm{CNR} = \frac{2 \cdot \left(\mu_{S_{ROI}} - \mu_{C_{ROI}}\right)^2}{\sigma^2_{S_{ROI}} + \sigma^2_{C_{ROI}}} \tag{3}$$

$$\mathrm{sSNR} = \frac{\mu_{S_{ROI}}}{\sigma_{S_{ROI}}} \tag{4}$$

where $\mu_{S_{ROI}}$ and $\mu_{C_{ROI}}$ are the average amplitude values in S_{ROI} and C_{ROI} (Fig. 5), respectively, while $\sigma_{S_{ROI}}$ and $\sigma_{C_{ROI}}$ represent the standard deviations.

A second numeric phantom, mimicking the left-ventricle, was also exploited to qualitatively assess the feasibility of tri-plane cardiac imaging. The position and amplitude of the scatterers were extracted from an open access database [22]; it is based on an electromechanical model and on a novel technique to compute scattering amplitudes so as to ensure realistic speckle patterns and image appearance.

III. Results

A. One-way fields

Fig. 4 and TABLE I summarize the comparison between SA and FA in terms of one-way field characteristics. SA and FA featured equivalent lateral resolution (2.4 mm) and DoF (37 vs 38 mm), but the gridded spiral presented worse GLL that were on average 5.6dB higher than those of the full-array. However, SA had a more uniform performance over the entire volume of interest, i.e. at all steering angles, since it showed a narrower standard deviation on GLL (0.9dB vs 3.7dB). Nevertheless, the limited number of elements of SA (200 vs 1024) impacted on the sensitivity that dropped by 13.7dB which is comparable to the expected value $20\log_{10}(1024/200) = 14.2$.

B. MLT Tri-plane imaging

Fig. 5 shows the simulated tri-plane images obtained from the anechoic cyst phantom. It highlights that, for both the probes, the images obtained on the 3 different planes are comparable. However, as previously shown in Fig. 4 and TABLE I, SA produced higher GLLs than FA; on the final tri-plane images, they corresponded to a 9.2dB lower CR (13.4dB vs 22.6dB) and to a 20% lower CNR (3.86 vs 4.82), as summarized in TABLE II. Qualitatively, the poorer contrast achieved with the SA corresponded to a reduction of the image dynamic range. Indeed, the anechoic inclusions shown on the right panels in Fig. 5 are filled in gray. On the other hand, the SA showed a marginal 7% improvement of sSNR (1.81 vs 1.68), thus a higher homogeneity of the background region.

Fig. 6 shows the simulated tri-plane images obtained in a more realistic scenario, i.e. on the left ventricle phantom. Qualitatively, it confirms that the quality obtained with SA is poorer compared to that obtained with FA; however, although stronger artifacts appear, especially inside the blood pool at the very first depths of interest, the walls of the left ventricle preserve sufficient contrast.

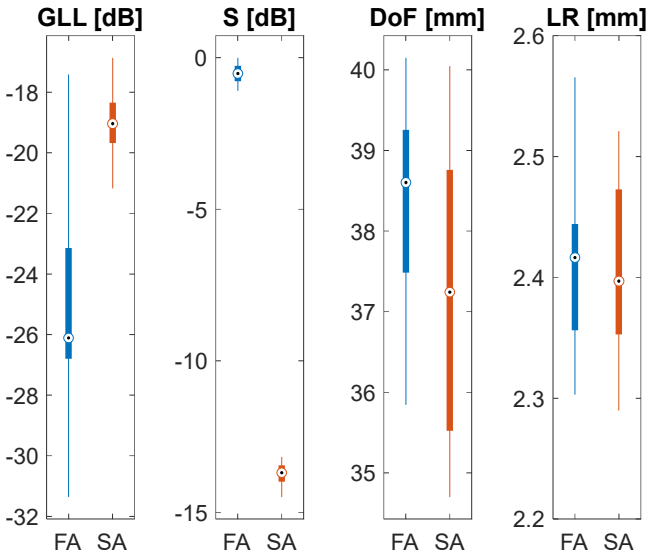

Fig. 4 Performance comparison on one-way fields: grating-lobe-level (GLL), sensitivity (S), depth of field (DoF), and lateral resolution (LR).

TABLE I
ONE-WAY FIELD PERFORMANCE METRICS

	GLL [dB]	S [dB]	DoF [mm]	LR [mm]
FA	−24.6±3.7	-0.5±0.3	38.4±1.2	2.42±0.07
SA	−19.0±0.9	−13.7±0.3	37.3±1.6	2.41±0.06

TABLE II
MLT TRI-PLANE IMAGING PERFORMANCE METRICS

	CR [dB]	CNR [A.U.]	sSNR [A.U.]
FA	22.6	4.82	1.68
SA	13.4	3.86	1.81

IV. Conclusion

In this work, we presented a feasibility study for MLT tri-plane cardiac imaging based on a sparse array. Simulations were conducted to compare the performance of a 1024-element, fully sampled, gridded array with a 200-element spiral array. We showed that, despite an unavoidable loss in image quality and sensitivity, due to a significant reduction of the number of elements (−80%), tri-plane imaging using MLT on a SA seems feasible. This would enable volumetric functional analysis of the heart using a system with low element and channel count.

References

[1] E. D. Light, S. F. Idriss, P. D. Wolf, and S. W. Smith, "Real-time three-dimensional intracardiac echocardiography," *Ultrasound Med. Biol.*, vol. 27, no. 9, pp. 1177–1183, Sep. 2001.

[2] L. Sugeng *et al.*, "Quantitative assessment of left ventricular size and function: side-by-side comparison of real-time three-dimensional echocardiography and computed tomography with magnetic resonance reference," *Circulation*, vol. 114, no. 7, pp. 654–661, Aug. 2006.

[3] S. Yagel, S. M. Cohen, I. Shapiro, and D. V. Valsky, "3D and 4D ultrasound in fetal cardiac scanning: a new look at the fetal heart," *Ultrasound Obstet. Gynecol.*, vol. 29, no. 1, pp. 81–95, Jan. 2007.

[4] A. Ortega *et al.*, "A Comparison of the Performance of Different Multiline Transmit Setups for Fast Volumetric Cardiac Ultrasound," *IEEE Trans. Ultrason. Ferroelectr. Freq. Control*, vol. 63, no. 12, pp. 2082–2091, Dec. 2016.

[5] P. Santos, J. Pedrosa, and J. Dhooge, "High frame rate multi-plane echocardiography using multi-line transmit beamforming: First experimental findings," in *2017 IEEE International Ultrasonics Symposium (IUS)*, 2017, pp. 1–1.

[6] Y. Chen, L. Tong, A. Ortega, J. Luo, and J. D'hooge, "Feasibility of Multiplane-Transmit Beamforming for Real-Time Volumetric Cardiac Imaging: A Simulation Study," *IEEE Trans. Ultrason. Ferroelectr. Freq. Control*, vol. 64, no. 4, pp. 648–659, Apr. 2017.

[7] L. Tong, H. Gao, and J. D'hooge, "Multi-transmit beam forming for fast cardiac imaging-a simulation study," *IEEE Trans. Ultrason. Ferroelectr. Freq. Control*, vol. 60, no. 8, pp. 1719–1731, Aug. 2013.

[8] L. Tong, A. Ramalli, R. Jasaityte, P. Tortoli, and J. D'hooge, "Multi-Transmit Beam Forming for Fast Cardiac Imaging: Experimental Validation and In Vivo Application," *IEEE Trans. Med. Imaging*, vol. 33, no. 6, pp. 1205–1219, Jun. 2014.

[9] A. Ramalli *et al.*, "Real-time high frame rate cardiac B-Mode and tissue Doppler imaging based on multiline transmission and multiline acquisition," *IEEE Trans. Ultrason. Ferroelectr. Freq. Control*, p. early access, 2018.

[10] B. Savord and R. Solomon, "Fully sampled matrix transducer for real time 3D ultrasonic imaging," in *2003 IEEE Ultrasonics Symposium (IUS)*, 2003, vol. 1, pp. 945–953.

[11] R. E. Davidsen, J. A. Jensen, and S. W. Smith, "Two-dimensional random arrays for real time volumetric imaging," *Ultrason. Imaging*, vol. 16, no. 3, pp. 143–163, Jul. 1994.

[12] A. Austeng and S. Holm, "Sparse 2-D arrays for 3-D phased array imaging - design methods," *IEEE Trans. Ultrason. Ferroelectr. Freq. Control*, vol. 49, no. 8, pp. 1073–1086, Aug. 2002.

[13] A. Austeng and S. Holm, "Sparse 2-D arrays for 3-D phased array imaging - experimental validation," *IEEE Trans. Ultrason. Ferroelectr. Freq. Control*, vol. 49, no. 8, pp. 1087–1093, 2002.

[14] B. Diarra, M. Robini, P. Tortoli, C. Cachard, and H. Liebgott, "Design of Optimal 2-D Nongrid Sparse Arrays for Medical Ultrasound," *IEEE Trans. Biomed. Eng.*, vol. 60, no. 11, pp. 3093–3102, Nov. 2013.

[15] A. Ramalli, E. Boni, A. S. Savoia, and P. Tortoli, "Density-tapered spiral arrays for ultrasound 3-D imaging," *IEEE Trans. Ultrason. Ferroelectr. Freq. Control*, vol. 62, no. 8, pp. 1580–1588, Aug. 2015.

[16] E. Roux, A. Ramalli, P. Tortoli, C. Cachard, M. C. Robini, and H. Liebgott, "2-D Ultrasound Sparse Arrays Multidepth Radiation Optimization Using Simulated Annealing and Spiral-Array Inspired Energy Functions," *IEEE Trans. Ultrason. Ferroelectr. Freq. Control*, vol. 63, no. 12, pp. 2138–2149, Dec. 2016.

[17] J. A. Jensen and N. B. Svendsen, "Calculation of pressure fields from arbitrarily shaped, apodized, and excited ultrasound transducers," *IEEE Trans. Ultrason. Ferroelectr. Freq. Control*, vol. 39, no. 2, pp. 262–267, Mar. 1992.

[18] J. A. Jensen, "FIELD: A Program for Simulating Ultrasound Systems," *Med. Biol. Eng. Comput.*, vol. 34, no. Supplement 1, Part 1, pp. 351–353, 1996.

[19] A. Ortega *et al.*, "HD-PULSE: High channel Density Programmable ULtrasound System based on consumer Electronics," in *2015 IEEE International Ultrasonics Symposium (IUS)*, 2015, pp. 1–3.

[20] E. Roux, A. Ramalli, H. Liebgott, C. Cachard, M. C. Robini, and P. Tortoli, "Wideband 2-D Array Design Optimization With Fabrication Constraints for 3-D US Imaging," *IEEE Trans. Ultrason. Ferroelectr. Freq. Control*, vol. 64, no. 1, pp. 108–125, Jan. 2017.

[21] C. Papadacci *et al.*, "Imaging the dynamics of cardiac fiber orientation in vivo using 3D Ultrasound Backscatter Tensor Imaging," *Sci. Rep.*, vol. 7, no. 1, p. 830, Apr. 2017.

[22] M. Alessandrini *et al.*, "A Pipeline for the Generation of Realistic 3D Synthetic Echocardiographic Sequences: Methodology and Open-Access Database," *IEEE Trans. Med. Imaging*, vol. 34, no. 7, pp. 1436–1451, Jul. 2015.

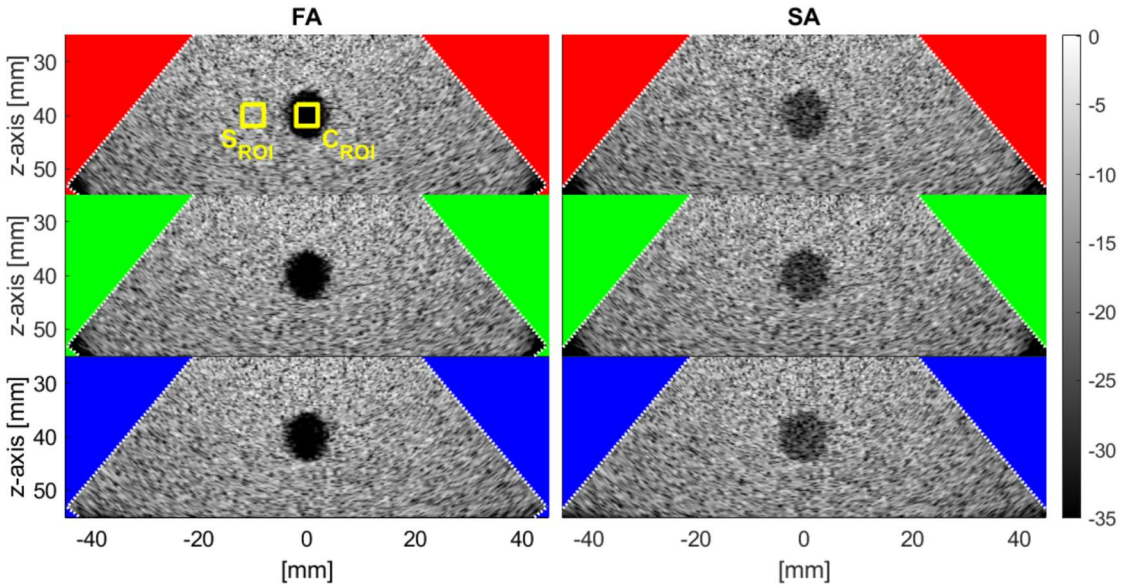

Fig. 5 Simulated tri-plane images of the numrical phantom obtained with both the FA (left) and the SA (right), reconstructed at different rotational angles 0° (red), 90° (green) and 45° (blu), respectively. In the top left panel, S_{ROI} and C_{ROI} indicate the regions of interest used to estimate the CNR, CR, and sSNR.

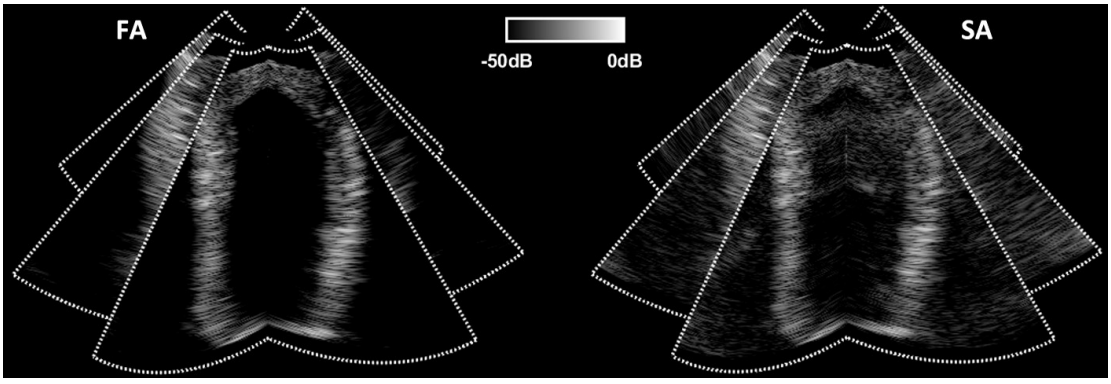

Fig. 6 Tri-plane images of the left ventricle phantom, obtained with FA (left) and SA (right).